Northumbria Research Link

Citation: Le, Bao, Kernin, Arnaud, Khaliq, Jibran, Fu, Guoyu, Huo, Dehong, Bilotti, Emiliano, Zhang, Han and Shyha, Islam (2021) Micro-End-Milling of Carbon Nanotube Reinforced Epoxy Nanocomposites Manufactured using Three Roll Mill Technique. Journal of Manufacturing Processes, 70. pp. 307-320. ISSN 1526-6125

Published by: Elsevier

URL: https://doi.org/10.1016/j.jmapro.2021.08.048 <https://doi.org/10.1016/j.jmapro.2021.08.048>

This version was downloaded from Northumbria Research Link: https://nrl.northumbria.ac.uk/id/eprint/47048/

Northumbria University has developed Northumbria Research Link (NRL) to enable users to access the University's research output. Copyright © and moral rights for items on NRL are retained by the individual author(s) and/or other copyright owners. Single copies of full items can be reproduced, displayed or performed, and given to third parties in any format or medium for personal research or study, educational, or not-for-profit purposes without prior permission or charge, provided the authors, title and full bibliographic details are given, as well as a hyperlink and/or URL to the original metadata page. The content must not be changed in any way. Full items must not be sold commercially in any format or medium without formal permission of the copyright holder. The full policy is available online: http://nrl.northumbria.ac.uk/policies.html

This document may differ from the final, published version of the research and has been made available online in accordance with publisher policies. To read and/or cite from the published version of the research, please visit the publisher's website (a subscription may be required.)

Northumbria University NEWCASTLE

University Library

Micro-End-Milling of Carbon Nanotube Reinforced Epoxy Nanocomposites Manufactured using Three Roll Mill Technique

Bao Le[a]*, Arnaud Kernin[b], Jibran Khaliq[a], Guoyu Fu[c], Dehong Huo[c], Emiliano Bilotti[b], Han Zhang[b], Islam Shyha[a, d]

[a]*Mechanical and Construction Engineering Department, Northumbria University at Newcastle, NE1 8ST, Newcastle upon Tyne, UK*

[b]*School of Engineering and Material Science, Queen Mary University, E1 4NS, London, UK*

[c]*Mechanical Engineering, School of Engineering, Newcastle University, NE1 7RU, Newcastle upon Tyne, UK*

[d] *School of Engineering and the Built Environment, Edinburgh Napier University, EH10 5DT, Edinburgh, UK*

**Corresponding author*

Keywords: nanocomposites, micro-end-milling, carbon nanotube, machinability

Abstract

Carbon nanotubes (CNTs) have been applied as nano-fillers to improve mechanical, thermal and electrical properties of polymers. Despite near net shape techniques could be used to manufacture nanocomposites, micromachining processes are still necessary to attain high surface quality and dimensional accuracy. Besides, micromachining of nanocomposites could be a potential approach to produce micro-features/components, following the miniaturisation trend of modern manufacturing. Therefore, micro-machining of these relatively new materials needs to be investigated. A comprehensive investigation on machinability of nanocomposites will be presented in terms of chip formation, cutting force, tool wear, surface morphology and surface roughness. Three controlled quantitative factors are investigated at different levels, including filler loading, cutting speed and feed per tooth (FPT). Micro-slotting is performed on an ultra-precision desktop micro-machine tool using uncoated carbide micro-end mill. The additions of multi-walled carbon nanotube (MWCNT) have shown significant effects on the machinability of these epoxy-based nanocomposites including a dramatic reduction in cutting force and machined surface roughness with accelerating tool wear compared with a neat polymer. The irregular cutting force variations when micro-milling epoxy/MWCNT nanocomposites at feed rates below minimum uncut chip thickness (MUCT) (lower than 2 µm) indicating by their fluctuations that different from those in higher feed rates. It possibly shows the impact of size effects that are illustrated by the observations of chip formation, surface morphology, cutting force profiles as well as specific cutting energy calculation.

1. Introduction

CNTs are allotropes of carbon that made of a cylindrical rolled-up single layer of carbon atoms. The diameters and lengths of CNTs typically range from 1-100 nm and 0.1 – 100 μm, respectively [1], with a high aspect ratio tubular structure and surface areas in the range of 200–900 m^2/g [2]. CNTs were discovered by Sumio Ijima in 1991 when examining the structure of carbon materials using an electron microscope [3], and the first single-walled carbon nanotube (SWCNT) was synthesised in 1993 by the same author [4]. Since their discovery, SWCNTs and MWCNTs are being used in different applications such as drug delivery [5], health care [6], electronics [7], and improving electrical and thermal properties of materials [8]. Most of these applications have used CNTs as a reinforcing agent in combination with polymers, especially epoxy. The commercial applications of epoxy reinforced with carbon fibre (CF), glass fibre (GF), Kevlar, or boron as structural materials have been found in many industrial areas such as aerospace [9], automotive industry [10], electronic packaging [11], wind turbine [12], or sport components [13]. Due to the high strength-to-weight ratio, thermal and electrical properties [14, 15], CNTs have been considered as a possible alternative to replace these conventional reinforcements in terms of fabricating light-weight polymer nanocomposites. However, the applications of CNT reinforced epoxy nanocomposites have been still limited despite many pieces of research on this field. These nanocomposites have been commercially utilised to manufacture hockey sticks, baseball bats [16], or components of nano-enhanced bikes [17]. Despite the substantial potential application, CNTs have been still currently used as a secondary reinforcing phase in carbon fibre reinforced polymer nanocomposites (CFRP) in all these commercial products. It is possibly due to the higher cost of CNTs compared to CF that prevented these nano-fibres from being applied in large structures [18]. Furthermore, the literature review from [19] showed that the primary barrier that limited the applications of CNT based nanocomposites was the synthesis optimisation. Uniform CNT distribution and CNT agglomeration have been still the main problems that reduce their reinforcing effectiveness of this nano-filler in polymer nanocomposites.

Micromachining of epoxy/CNT nanocomposites showed high potential to be applied in manufacturing of micro-components due to the miniaturisation demands of modern manufacturing [19, 20] such as micro-electronics [21], micro-mechanical devices [22]. Although many near-net-shape methods such as micro-moulding, lithography have been employed to manufacture CNT reinforced polymer nanocomposites, mechanical micromachining techniques (i.e. micro-drilling, micro-turning or micro-milling) are deemed to be necessary to provide sufficient quality of machined surface or dimensional accuracy as post-processes. However, micromachining of nanocomposites seemed to be a complicated process due to the anisotropic, heterogeneous structure of workpiece materials [20] and thermo-mechanical reinforcements of nano-filler [23]. Furthermore, research into nanocomposites micromachining will be able to fill in the gap between macro and micromachining, namely “size effect”. This physical phenomenon exhibits by the combinations of various effects including cutting edge radius, microstructure, and minimum uncut chip thickness [20]. As a result, it became necessary to investigate the micromachining behaviours of these polymer nanocomposites while taking into account the size effect.

Despite the vast potential of epoxy/CNT micromachining, most studies in this field have have focused on MWCNT reinforced polycarbonate (PC/MWCNT) [24], MWCNT reinforced polystyrene (PS/MWCNT) [25], or graphene and MWCNT reinforced PC (PC/graphene/MWCNT) nanocomposites [26]. There were also some researchers investigated the machinability of graphene reinforced epoxy nanocomposites [27, 28]. However, no research was found to be done on epoxy/CNT nanocomposite micromachining. Furthermore, the size effect when micromachining polymer nanocomposites has also not been thoroughly investigated. Therefore, this paper aimed to provide a comprehensive investigation on micro-machinability of

epoxy/MWCNT nanocomposite. The micromachining experiments were conducted on different cutting conditions (feed per tooth, cutting speed) and MWCNT filler loadings at a constant axial depth of cut of 200 µm in dry cutting condition. The main objectives included cutting force and surface roughness. Additionally, the investigations on chip morphology, machined surface morphology were addressed to support the analysis of these two main machinability indicators. Tool wear behaviour of micro-cutting tools at the end of the micro-milling trials (for each composition and plain epoxy) was also addressed to assess the effect of MWCNT loading on this category. Additionally, low feed per tooth (0.2 and 0.5 µm) were also employed to investigate the size effect in polymer nanocomposites micromachining. Besides, material properties including tensile mechanical properties and thermal conductivity were supposed to have considerable influences on the machinability of epoxy/MWCNT nanocomposites in micro-milling, hence characterised before the micromachining trials.

2. Experimental work

2.1 Materials synthesis

Epoxy nanocomposites with various MWCNT loadings (0.1, 0.3, 0.5, 0.7 and 1 wt.%) were synthesised using a two-component epoxy system as a matrix having epoxy resin RX771C and epoxy hardener HX932C, both supplied by Robnor Resinlab, UK. MWCNTs (NC7000TM (purchased from Nanocyl Inc., Belgium) had an average diameter of 9.5 nm, average length ~ 1.5 µm, density of 1.66 g/cm^{3,} and surface area around 250-300 m^2/g.

The mixtures of MWCNT and epoxy resin were first prepared by manual mixing for 5 minutes. A three-roll mill (TRM) (80E EXAKT GmbH, Germany) was then used to incorporate nanotubes into epoxy resin. After homogenous mixtures of MWCNT and epoxy resin were attained by TRM, they were manually mixed with epoxy hardener (HX932C) for 5 minutes. Subsequently, these mixtures were degassed in a vacuum chamber (pressure of - 1 bar) at 50^{o}C for 1 hour, while stirring (with a magnetic stirrer), before poured into silicone moulds at room temperature. The mixture was then cured in an oven at 120 °C for 12 hours, as recommended by the supplier (Robnor Resinlab) to attain full crosslinking of epoxy.

2.2 Characterisation of MWCNT/EP nanocomposite

The standard ASTM D638 test method was selected to conduct the characterisation of the tensile properties of nanocomposites. Tensile tests were conducted on a Universal Testing machine (INSTRON 3382) to characterise the tensile behaviour (tensile strength, Young's modulus and fracture strain) of all epoxy/MWCNT nanocomposites and plain epoxy. Following the ASTM D638 standard, the type V specimen prepared by moulding had the dimension shown in Figure 1.

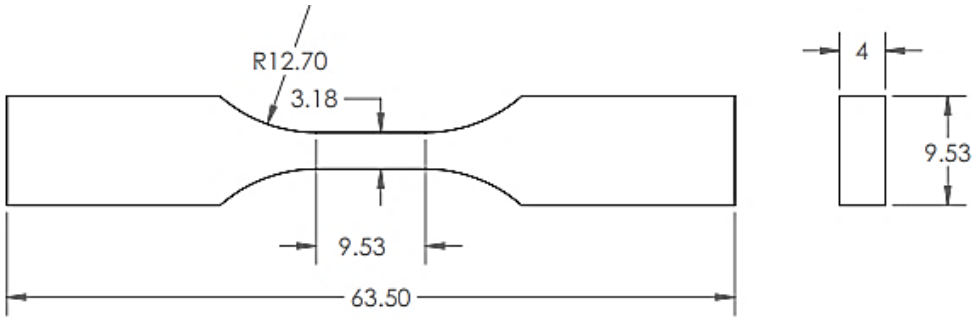

Figure 1: Tensile test specimen, type V geometry (ASTM D638) (Unit: mm)

ASTM D5470 standard was employed to measure the thermal conductivity of epoxy/MWCNT. The linear heat conduction tests were performed on Hilton H112A device. The characterisation set up of thermal conductivity and dimensions of the sample are shown in Figure 2.

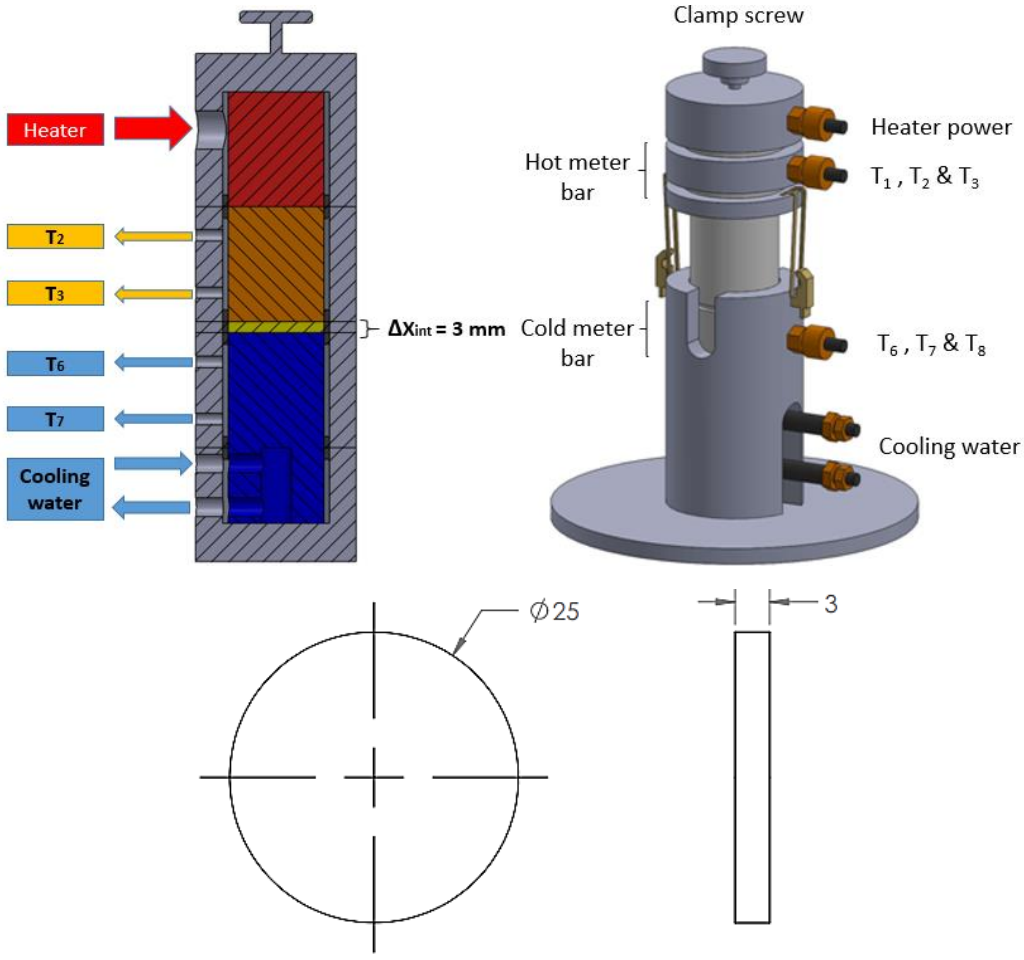

Figure 2: Thermal conductivity test setup on Hilton H112A linear heat conduction (ASTM D5740) with the dimensions of specimens (unit: mm)

Five specimens were used for each composition (including plain epoxy) for both tensile and thermal conduction tests. One measurement was performed on each sample and the

average values were used to indicate the magnitudes of tensile properties (i.e., tensile strength) and thermal conductivity.

2.3 Micromachining experiments

Micro-end milling experiments were performed on an ultra-precision desktop micro-machine tool (Nanowave MTS5R). High-speed cutting in micromachining was attained by using high-speed spindle with a max speed of 80,000 rpm. The spindle contained air spindle to minimise the vibration during the cutting process. This spindle can provide an output torque of 3 cNm in the speed range from 20,000 to 80,000 rpm. A precision of 0.1 µm can be attained using XYZ slideways. The experimental setup is shown in Figure 3, which includes nanocomposite specimen, main spindle, micro-end mill and dynamometer. Besides, the high rigidity of the machine stage also allowed stable operations during micromachining process at such a low feed rate (0.1 µm). Full immersion micro-milling was applied for all cutting trials with a constant axial cutting depth of 200 µm in dry condition. The micro-end milling uncoated tools used in this study (Kyocera 1610-0197.059) had some main features as follows: micro-grain tungsten carbide, two flutes, cutting diameter of 0.5 mm and helix angle of 20^0. Ultra-precision collets were also employed to minimise the adverse effects of tool runout (below 1 µm). However, this threshold could be further reduced with adjustment.

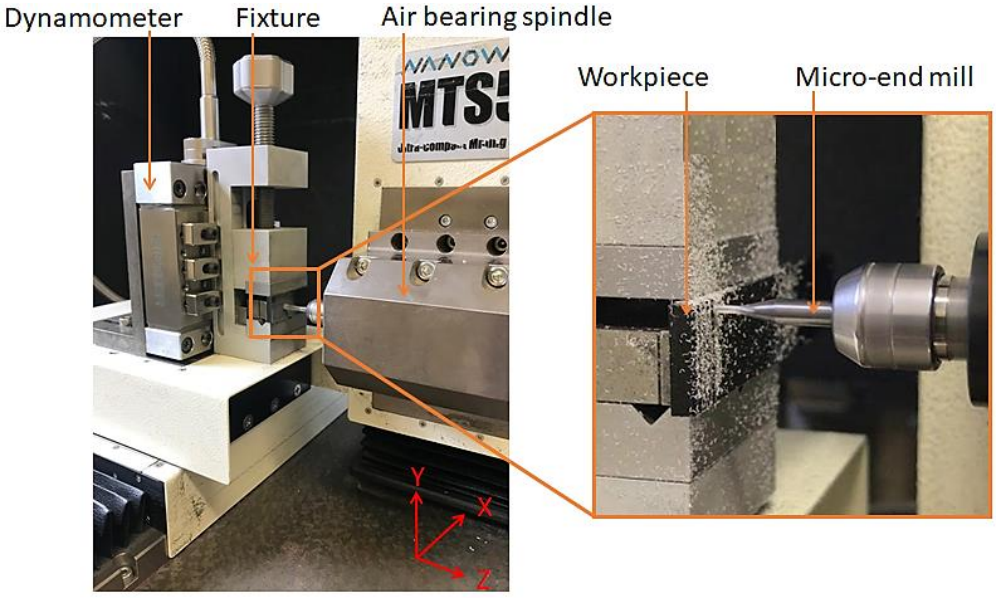

Figure 3: Experimental setup for the micro-milling trials

Following the manufacturing of epoxy/MWCNT loaded with various CNT contents using three roll milled technique, the study aimed to investigate the effect of three controlled quantitative factors including CNT loading, feed rate and cutting speed when micro-end-milling. Each test at every specific condition was repeated three times. The dimensions of machining specimens were 70 x 13 x 3 mm (Length x Width x Thickness). The experimental plan is shown in Table 1. The selected values for the process parameters were based on the literature and the capability of the machine tool in terms of attaining stable cutting conditions

at low cutting chip load or high cutting speed. The experimental results of micro-milling neat epoxy specimens were also collected and compared to other compositions.

Table 1: Experimental settings

Specimen	Material	MWCNT reinforced epoxy and plain epoxy
	Dimension (L x W x T) (mm)	70 x 13 x 3
	Filler loading (wt%)	0, 0.1, 0.3, 0.7 and 1.0
Cutting tool	Material	Micro-grain tungsten carbide
	Type	Uncoated micro-end mill
	Number of flutes	2
	Flute length (mm)	1.5
	Cutting diameter (mm)	0.5
	Helix angle	20^0
Cutting conditions	Cutting speed (m/min) (rpm)	62.8 (20,000), 125.6 (40,000) and 188.5 (60,000)
	Feed per tooth (µm)	0.2, 0.5, 1, 2, 4
	Axial depth of cut (DoC) (µm)	200
	Cutting width (µm)	0.5
	Cutting length (mm)	13

Kistler (9256C2) piezoelectric dynamometer with high frequency (up to 4.8 kHz) and large measuring range (-250 to 250 N) was attached behind the fixture to measure the micro-cutting forces in *x*, *y*, and *z* directions. In this case, *Fy* was the feed force *(F_f)* and was measured in the feed direction of the tool. *Fx* was the feed normal force (F_{fn}) (perpendicular to F_f), while F_z was the passive cutting force (F_p) (axial to the central tool line) (Figure 4a). The signals generated from the force sensor were conducted into the charge amplifier (Kistler 5070A) (Figure 4b). Based on that, resultant cutting forces were calculated using the formula below:

$$F = \sqrt{F_x^2 + F_y^2 + F_z^2}$$

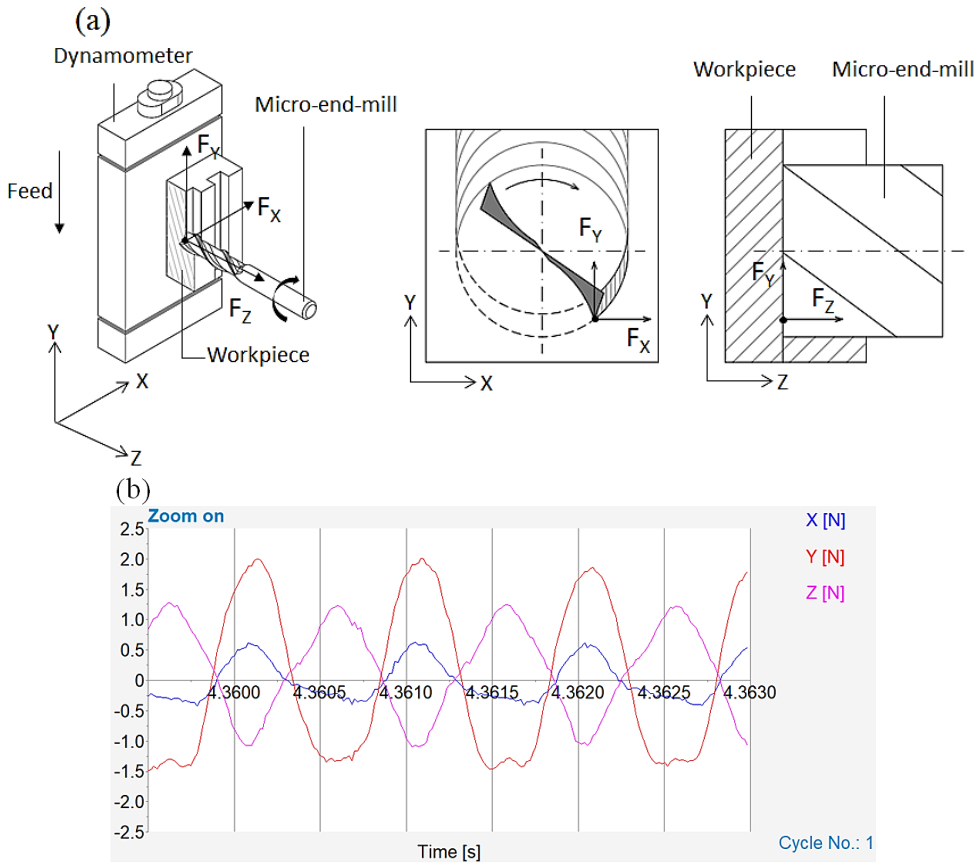

Figure 4: (a) Schematic representing cutting force measurement in micro-milling and (b) Typical cutting force signals during micro-milling process

A scanning electron microscope (SEM) TESCAN MIRA3 was used to investigate tool wear. The geometry of new tools was first considered by SEM imaging. Due to the unobvious tool wear for each cutting condition (three trials), it was unlikely to have considerable effect on the machining process. Therefore, the observation on tool wear was made after finishing every CNT loading or 45 trials (replicated three times at five levels of FPT and three levels of cutting speed). The cutting volume of each composition was 58.5 mm^3. The non-uniform flank wear (VB 2) and the stair-formed face wear (KT 2) were used as the main criteria tool wear assessment that were based on ISO 8688-2 standard [29]. The flank wear VB2 was the maximum bandwidth in the perpendicular direction to the original cutting edge on the side view (Figure 5). The face wear KT 2 occurred at the intersection of the wear scar and the major flank surface was measured perpendicular to the tool face (Figure 6).

All used tools were from the same batch to minimise manufacturing errors. SEM was also employed to investigate the surface morphology as well as the microstructure of the specimens after micro-milling. Surface roughness Ra was measured based on ISO 4287-1997 standard [30] (contact-based measurement) using a profilometer Mitutoyo Surftest SJ-410 (0.25 mm and 2.5 mm cut off and measurement length, respectively). The chips from the micro-milling processes at each cutting condition were collected using carbon tape. The chip morphology was then investigated using SEM analysis.

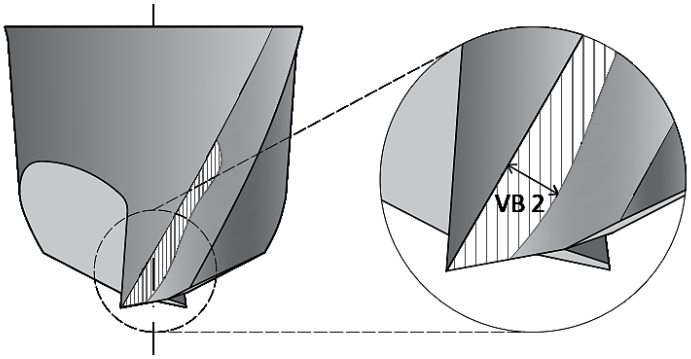

Figure 5: Non-uniform flank wear measurement

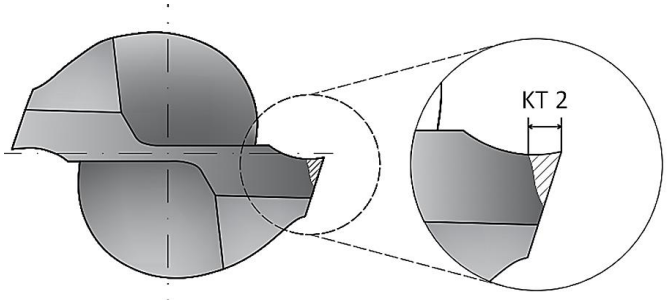

Figure 6: Stair-formed face wear measurement (with the original cutting-edge outline)

Based on the experimental results of cutting force and surface roughness, Analysis of Variance technique (ANOVA) was applied to analyse these experimental data as well as identify the most significant factor (i.e., cutting speed, FPT, filler content) that affects the machinability.

Furthermore, the specific cutting energy was also calculated to validate the size effect when micromachining at FPT below MUCT. This indicator was considered as the cutting energy consuming for a volume unit of material removal. It could be identified by using the equation below:

$$E = \frac{Cutting\ energy}{MRR} = \frac{F.V}{w.D.V_f}$$

Where:

- E: Specific cutting energy (J/mm3)
- F: Resultant cutting force (N)
- V: Cutting speed (m/min)
- W: Width of cut (mm)
- D: Depth of Cut (mm)
- V_f: Table feed (mm/min)
- MRR: Material removal rate (mm^3/min)

3. Results and discussion

3.1 Tensile properties

The tensile properties of nanocomposites with different MWCNT contents are shown in Figure 7(a-c). The addition of varying filler contents, from 0.1 to 1 wt.%, significantly affected the tensile behaviour of epoxy-based nanocomposites. It could be observed that both tensile strength (Figure 7a) and Young's modulus (Figure 7b) were improved when adding more MWCNT into epoxy matrix compared to the plain epoxy that were consistent with the literature [31]. These improvements were possibly contributed by the homogeneous distribution of MWCNTs generated from using TRM. Furthermore, it could also be seen that the fracture strain of these nanocomposites (Figure 7c) increased when incorporating MWCNT from 0 to 0.3 wt.%. However, it started to decrease when the filler loading reached 0.7 wt.%, indicating a ductile-to-brittle transition. This phenomenon was possibly due to more agglomerations of MWCNT at high filler content, generating more stress concentration, hence leading to crack propagations under tensile loadings. Some similar findings could be found in [31, 32]. The improvements of tensile strength and modulus combined with the decrease of strain failure could be used to explain the effects of filler content on the machinability of these nanocomposites (i.e., cutting force, surface roughness, chip formation) [19]. Furthermore, the thermal conductivity of these nanocomposites should also be considered since it could also influence the micromachining process in particular when thermal softening phenomenon was dominant (at high cutting speed). Therefore, the thermal characterisation of epoxy/MWCNT nanocomposites was expressed in section 3.2.

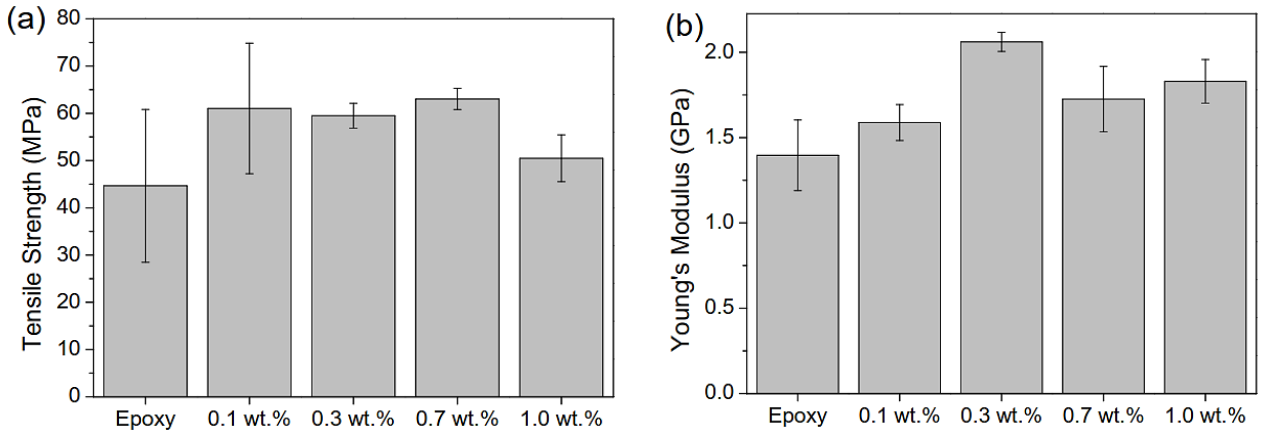

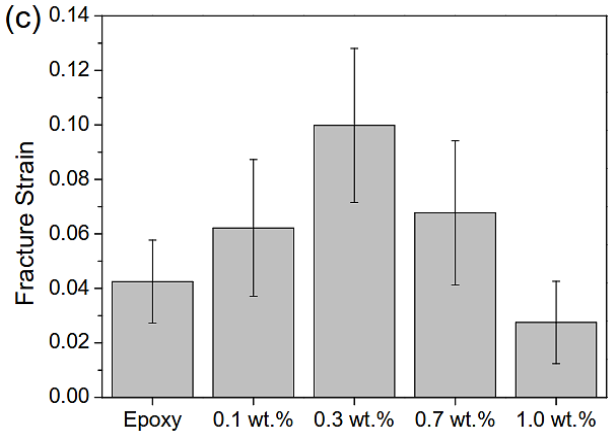

Figure 7: Tensile properties of epoxy/MWCNT nanocomposites: (a) Tensile strength, (b) Young's modulus, and (c) Fracture strain

3.2 Thermal conductivity

Since the cutting process generated high temperature in the cutting zone, causing workpiece material softening and chip adhesion that might affect the surface quality and surface roughness. In micromachining, high cutting speed is preferred, so this phenomenon was expected to be more severe. Therefore, micromachining low-thermal-conductivity materials, such as polymers, required the investigation on their thermal conductivity. The thermal conductivity of epoxy/MWCNT nanocomposites is shown in Figure 8. A slight improvement could be observed when the filler content reached 0.7 wt.%. The highest thermal conductivity value was found for 1 wt.% MWCNT, which was in a reasonable agreement with other studies [33, 34]. These enhancements of thermal conductivity was possibly due the heat flow formed by dense MWCNTs network inside epoxy matrix at high filler contents (0.7 and 1 wt.%) as reported in the literature [35].

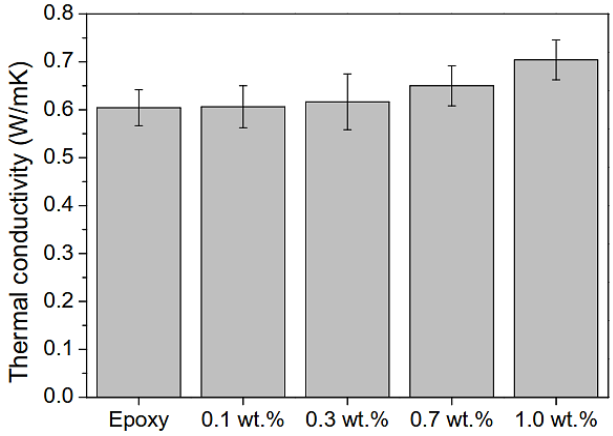

Figure 8: Thermal conductivity of epoxy/MWCNT nanocomposites at different filler contents

3.3 Chip morphology

The chip morphology in micromachining plays a vital role in identifying the cutting mechanism as well as the behaviours of workpiece materials under the cutting process. In this section, the morphology of chips from different material compositions and cutting conditions was investigated. It was expected that feed rate and filler content would show apparent influences on the chip formation due to the improvements of tensile properties and thermal conductivities of nanocomposites. Additionally, more details of chip morphology at low feed rates were also analysed to identify the minimum uncut chip thickness (MUCT). This was indicated by a transition point from ploughing to the shearing-dominated regime and was an essential indicator of size effect when micromachining.

Figure 9 shows the chip morphology characterisation at a cutting speed of 62.8 m/min for different filler contents and FPT. Using such low magnification (200x) in this case can provide a general view of different chip morphologies as the FPT increased. For all compositions, the chips were transferred from discontinuous to continuous forms when increasing the feed rate. It indicated the transition of cutting mechanism from ploughing into shearing. However, this trend seemed to be different between each composition. For plain epoxy, 0.1 wt.% and 0.3 wt.% MWCNT nanocomposites, the chips were crushed with fracture debris at lowest FPT of 0.5 µm and became more noticeable but still was in discontinuous form when FPT reached to 1 µm. For 0.7 wt.% and 1 wt.% MWCNT nanocomposites, the chips were much more apparent, even at 0.5 µm FPT.

Furthermore, the chip transition points from discontinuous to continuous form in these higher filler content nanocomposites were between 0.5 and 1 µm, which were smaller than those of lower filler contents and plain counterparts (from 1 to 2 µm). Since the chip formation was characterised at the lowest cutting speed (62.8 m/min), the effect of thermal softening could be eliminated. Tensile behaviour of these materials would be considered as the main reason for the change of MUCT between them. Based on the stress-strain curves in Figure 7, it could be seen that the reduction of failure strain seemed to reduce the MUCT when micromachining high-filler-content nanocomposites. It made the shearing mechanism dominant even at a low feed rate. On the contrary, ploughing predominated when micromachining lower filler content nanocomposites due to their viscoelastic behaviour. Therefore, the addition of different MWCNT contents likely changed the MUCT thresholds when micro-milling epoxy/MWCNT nanocomposites, owing by their various tensile behaviours.

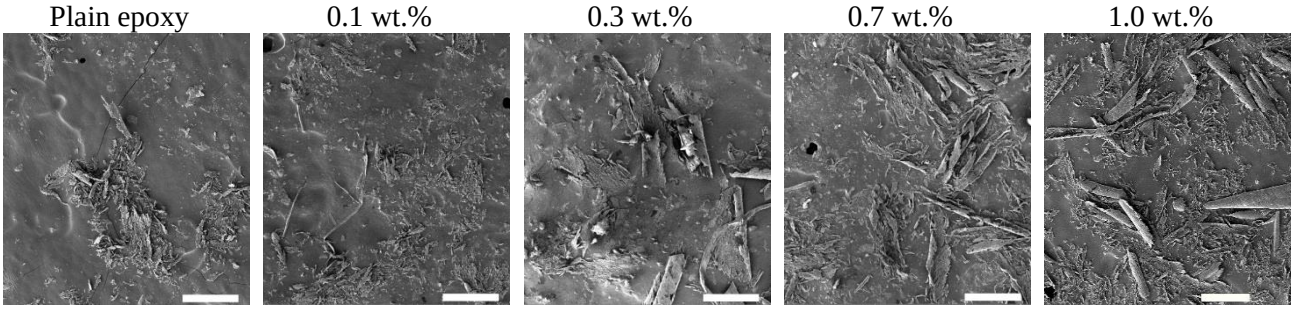

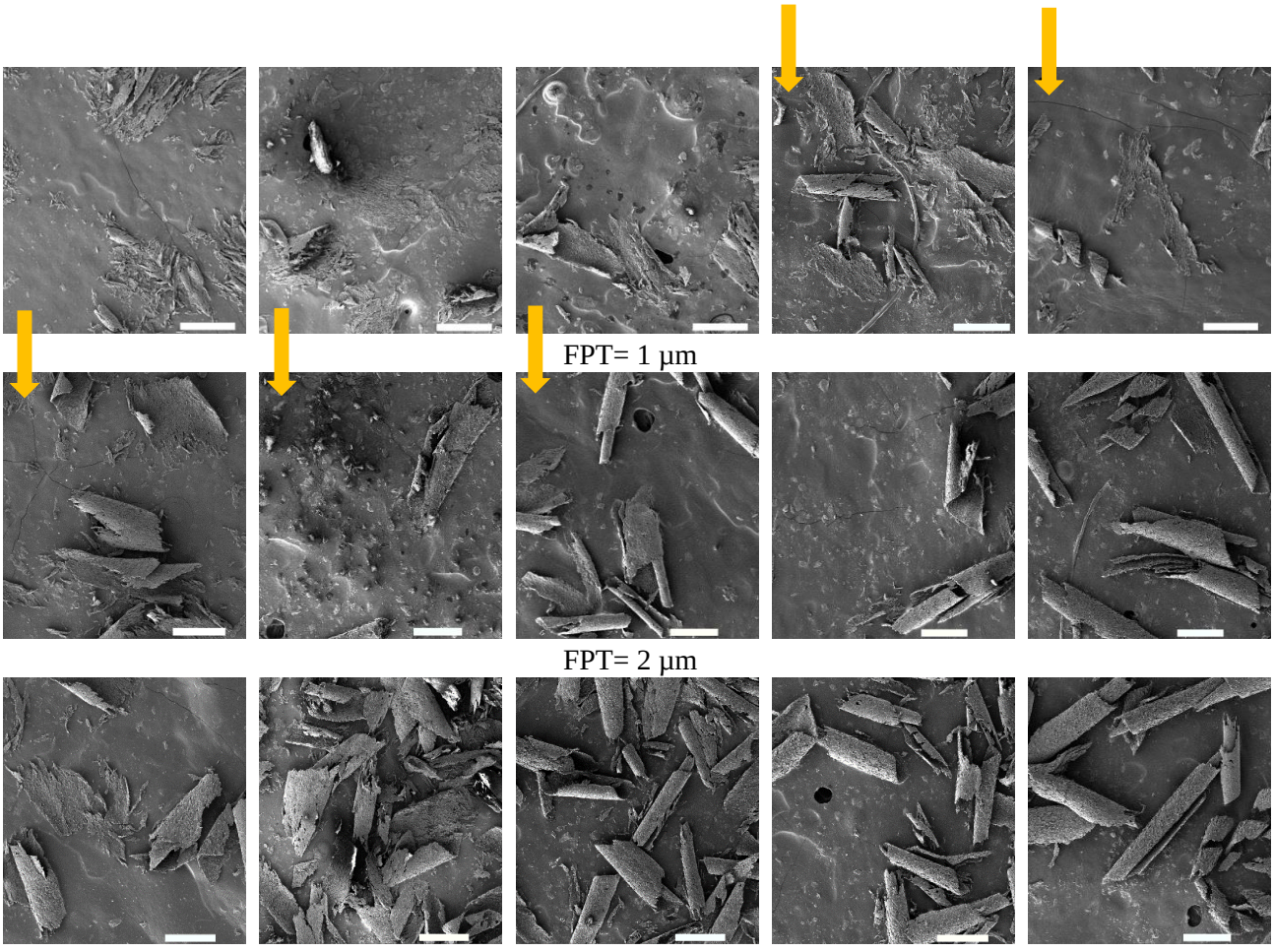

Figure 9: Chip formations when micro-milling at different FPTs and CNT weight contents (Cutting speed = 62.8 m/min; Scale bar is 200 µm)

In this case, MUCTs of 0.7 wt.% and 1 wt.% MWCNT nanocomposites were in the range of 0.5 - 1 µm) while these values were from 1 to 2 µm in case of low-filler-content nanocomposites. On closer observation of chip formations at low feed rates (Figure 10), it could be seen that chip formation of 0.7 and 1 wt% MWCNT nanocomposites were continuous and partly discontinuous at lowest FPT of 0.2 µm indicating a partial shearing-dominant regime. At the same time, a completed ploughing mechanism was dominant at lower filler contents. At FPT of 1 µm, the chips of higher filler content nanocomposites were likely to curl and become thicker. However, their chip surfaces were rough with the presence of micro-cracks, possibly due to low tensile strain-to-failure behaviour of nanocomposites at high filler contents that has been confirmed from the tensile results.

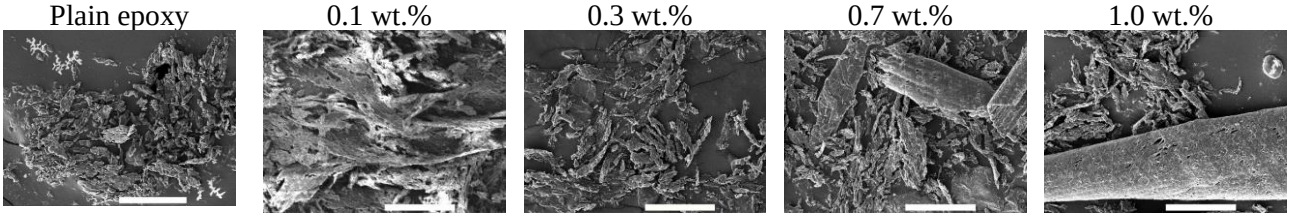

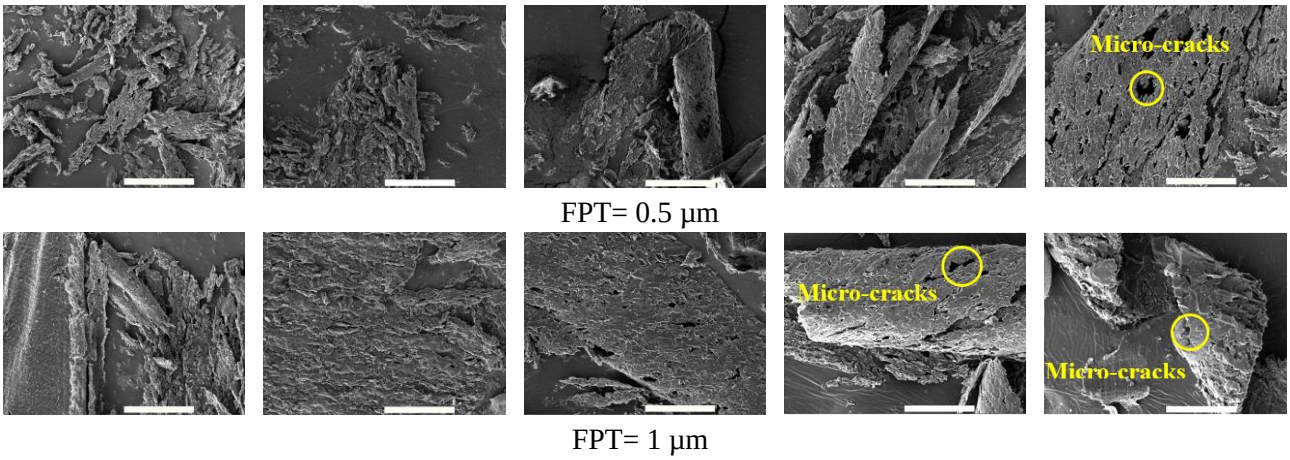

Figure 10: Chip formations at low FPTs at different CNT weight contents (Cutting speed = 62.8 m/min; Magnification = 1.5kx; Scale bar length is 50 µm)

3.4 Cutting Force

In micromachining nanocomposites, cutting force response seemed to be more sensitive with the changes of cutting conditions and filler content due to the utilisation of high cutting speed, low feed rate, the complex microstructure of nanocomposites and micro-cutting tool. Therefore, this machinability indicator was likely imperative for micromachining mechanics study.

Firstly, ANOVA was applied based on the cutting force results from all cutting conditions and filler contents at a significance level (α) of 0.05. Table 2 depicts all input factors, including filler content, cutting speed and FPT with their levels of effects on cutting force representing as contribution indicators. The filler content and FPT showed the most significant influences with their contributions to cutting force variation of ~ 30% and ~ 32%, respectively as well as their low P-values (<0.001). The cutting speed only marginally influenced cutting force (2.76%).

Table 2: ANOVA result for cutting force when micro-milling epoxy/MWCNT nanocomposites

Source	DF	Seq SS	Contribution	Adj SS	Adj MS	F-Value	P-Value
Filler Content (wt.%)	4	3.5764	30.03%	3.5764	0.89409	13.79	< 0.001
Cutting Speed (m/min)	2	0.3285	2.76%	0.3285	0.16425	2.53	0.087
FPT (µm)	4	3.8542	32.37%	3.8542	0.96356	14.86	< 0.001
Error	64	4.1491	34.84%	4.1491	0.06483		
Total	74	11.9082	100.00%				

Figure 11 shows the variations of cutting force as a function of FPT when a micro-milling epoxy/MWCNT nanocomposite at different cutting speeds. A gradual increase of cutting force along with feed rate increment was observed for all cutting speeds. Micro-

milling 1 wt.% MWCNT generated highest cutting force regardless of the cutting conditions. However, its cutting force magnitude was highest and sharper increase could be seen at 62.8 m/min compared to those of other compositions (Figure 11a). These results possibly indicated the dominance of mechanical strengthening effect at low cutting speed. At higher cutting speeds, this phenomenon became less evident due to the interferences of thermal softening and microstructure effects. The cutting forces when micro-milling other compositions at 62.8 m/min showed comparable magnitudes at FPT below 2 µm. However, the influence of filler content and, consequently, strengthening effect became more evident at higher FPTs.

The ploughing tended to dominate the cutting mechanism in this domain. The effect of filler content on cutting force was most apparent when micromachining at the highest cutting speed of 188.5 m/min (Figure 11b). It was expected that heat generation from milling at such high cutting speed would make the thermal softening more sensitive, especially with low-thermal-conductivity materials such as plain epoxy, 0.1 wt.% and 0.3 wt.% MWCNT nanocomposites. Therefore, it seemed to have a fundamental difference between micromachining lower and higher thermal conductivity materials (0.7 wt.% and 1 wt.% MWCNT nanocomposites) in this case. While a mechanical strengthening-dominant regime could be seen at high filler content, the thermal-softening effect seemed to occur at the rest. It led to the most obvious influence of MWCNT content on cutting force at the highest cutting speed.

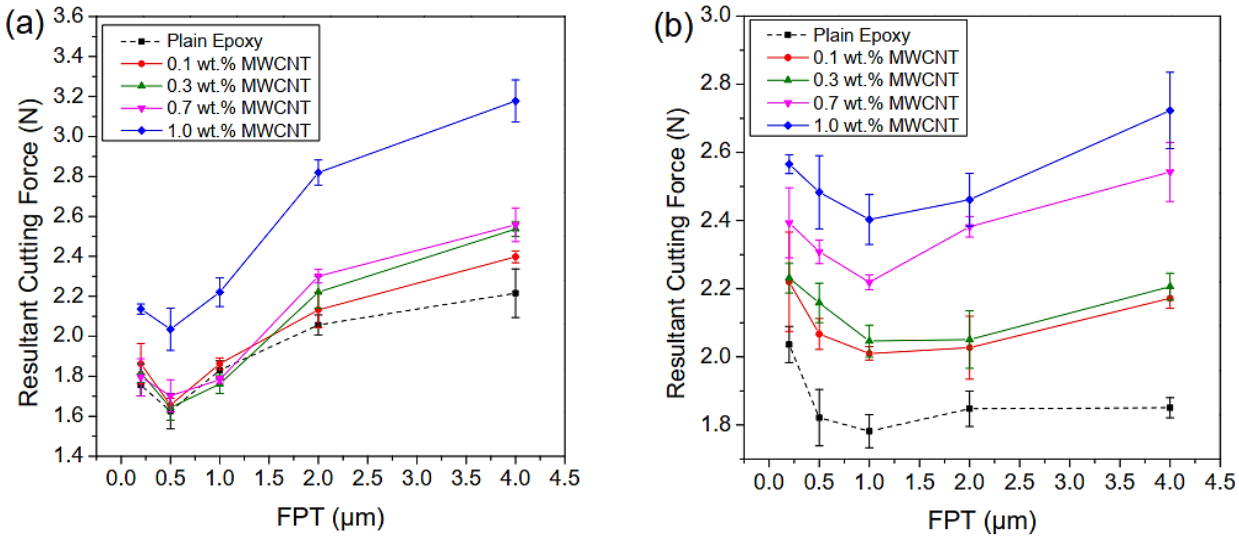

Figure 11: Cutting force when micro-milling epoxy based nanocomposites at different MWCNT contents and FPTs: a) Cutting speed = 62.8 m/min (20,000 rpm); b) Cutting speed = 188.5 m/min (60,000 rpm)

Micromachining at low FPT (0.2 - 1 µm) showed a distinct trend compared to others for all cutting speeds. Instead of increasing along with feed rate, cutting forces were high at the beginning and then fluctuated within this low range of FPT. It again confirmed the predominance of the size effect in this region while micromachining at feed rate below MUCT boundary. The ploughing or partial shearing made the cutting force variation complicated. Additionally, this domain seemed to be larger (from 0.2 to 2 µm) as the highest cutting speed

was employed due to thermal softening effect. Figure 12 depicts some specific cutting profiles on feed direction (F_y) at cutting speed of 62.8 m/min to clarify the MUCT effect on cutting force variation for FPT of 0.5 and 1 µm. The influence of microstructure could be eliminated at such low cutting speed. The cutting force profile appeared to be irregular at FPT of 0.5 µm regardless of the material type. However, cutting profile at 1 wt.%, MWCNT seemed to have most regular fluctuation compared to other compositions that indicate a certainly regular shearing, even at low FPT. When 1 µm FPT was employed, only micromachining of 0.7 wt.% and 1 wt.% MWCNT nanocomposite achieved regular cutting profiles. In contrast, others still kept non-uniform, indicating a lower MUCT for high-filler-content materials at around 0.5 - 1 µm. This result was likely to confirm the MUCT identification that was found in the chip morphology section (section 3.3) (Figure 9).

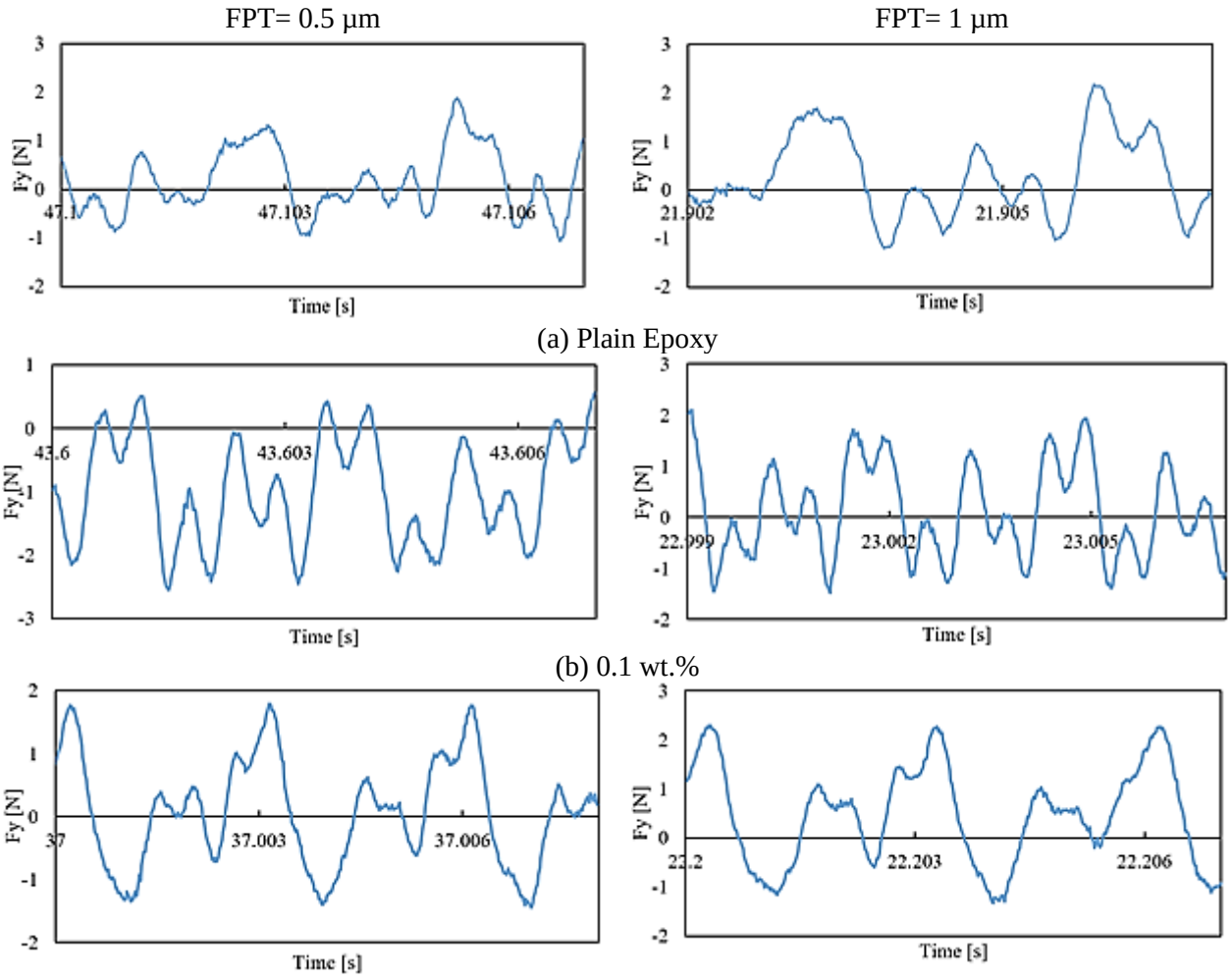

(a) Plain Epoxy

(b) 0.1 wt.%

(c) 0.3 wt.%

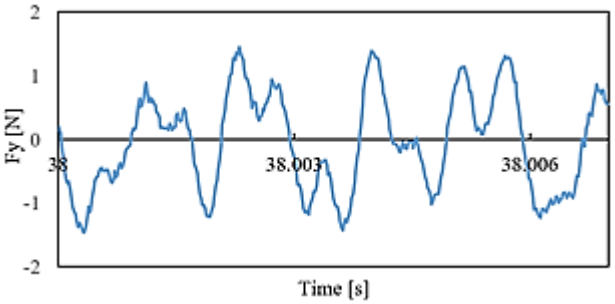

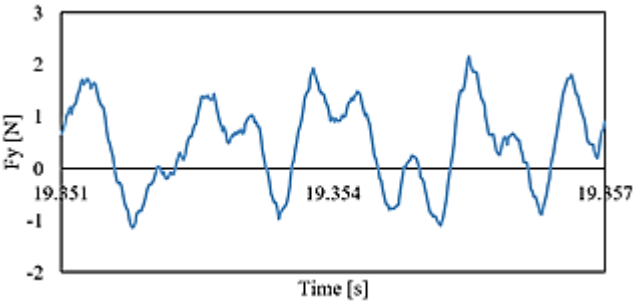

(d) 0.7 wt.%

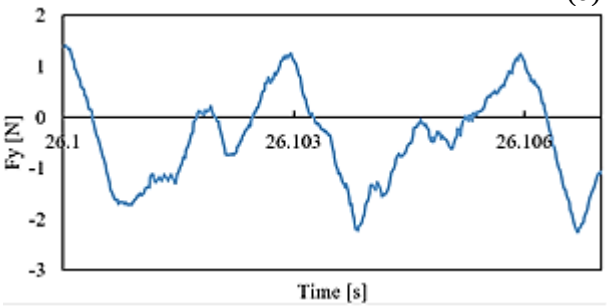

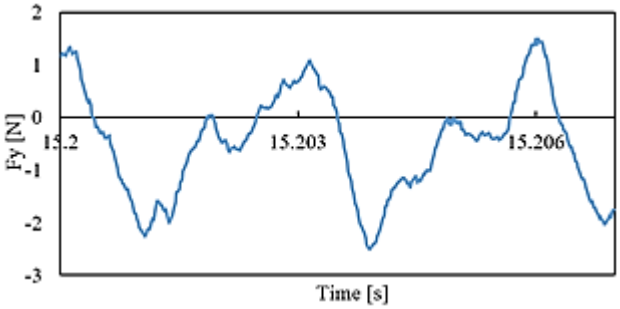

(e) 1.0 wt.%

Figure 12: Cutting force profiles in feed direction at low FPT (0.5 and 1 µm) (Cutting speed= 62.8 m/min)

3.5 Specific cutting energy

Figure 13 shows the variation of the specific cutting energy when micro-milling different material compositions at the cutting speed of 62.8 m/min and the axial depth of cut of 200 µm. A rapidly non-linear increase of the specific cutting force as FPT decreased below MUCT threshold could be observed for all materials. The cutting process likely underwent ploughing-dominant mechanism, making elastic deformation of material rather than being sheared at this FPT range. As a consequence, the specific cutting energy at FPT of 0.2 µm reached to highest values, especially for 1 wt.% MWCNT nanocomposite.

On the contrary, micromachining as FPT beyond MUCT appeared to achieve stable material removal mechanism as their specific cutting energy gradually reducing at lower magnitudes. Shearing regime was likely predominant, leading to plastic deformation of the material. This claim could be confirmed by the chip morphology observation in the previous section (section 3.3) with discontinuous chips at low FPTs and became more continuous and curlier as FPT increasing.

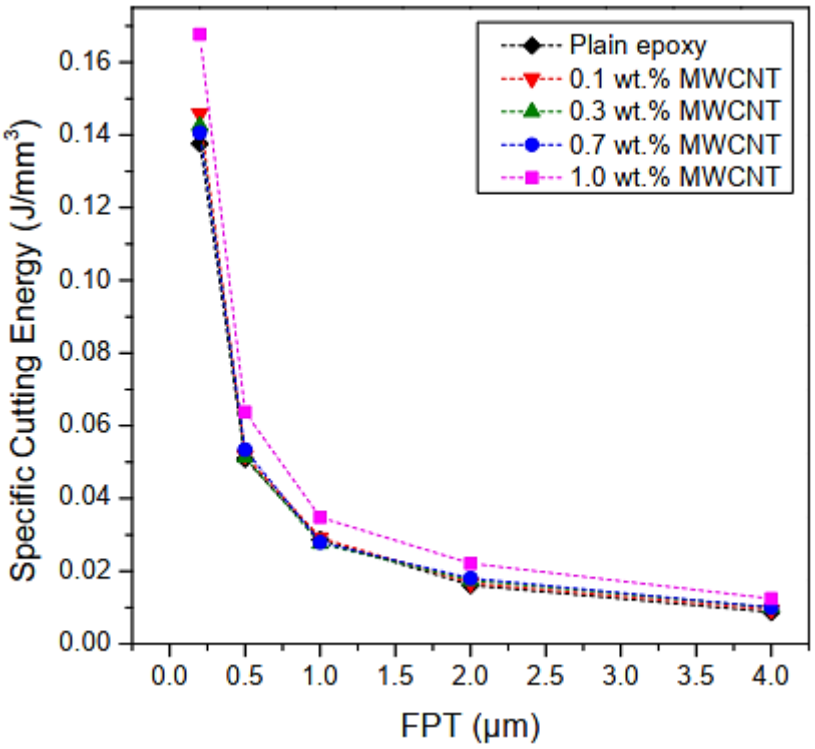

Figure 13: Specific cutting energy when micro-milling at different MWCNT contents (Cutting speed = 62.8 m/min)

3.6 Machined surface morphology

Figure 14 shows general views of machined surface morphology at low magnification of 750x (cutting speed of 62.7 m/min and FPT of 4 μm). These SEM images have been captured at the central area of each slot. It was observed that the presence of feed marks becomes more pronounced when micro-milling high-content-filler nanocomposites. It was possibly due to lower failure strain as high filler loadings are used. The feed marks on machined surfaces of plain epoxy and lower filler content nanocomposites seemed to be smeared by the matrix material due to their visco-elastic characteristic. It was likely compatible with the tensile characterisation of these materials.

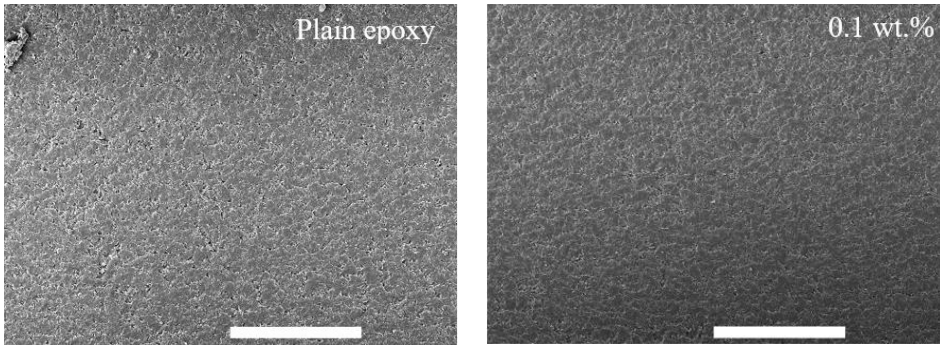

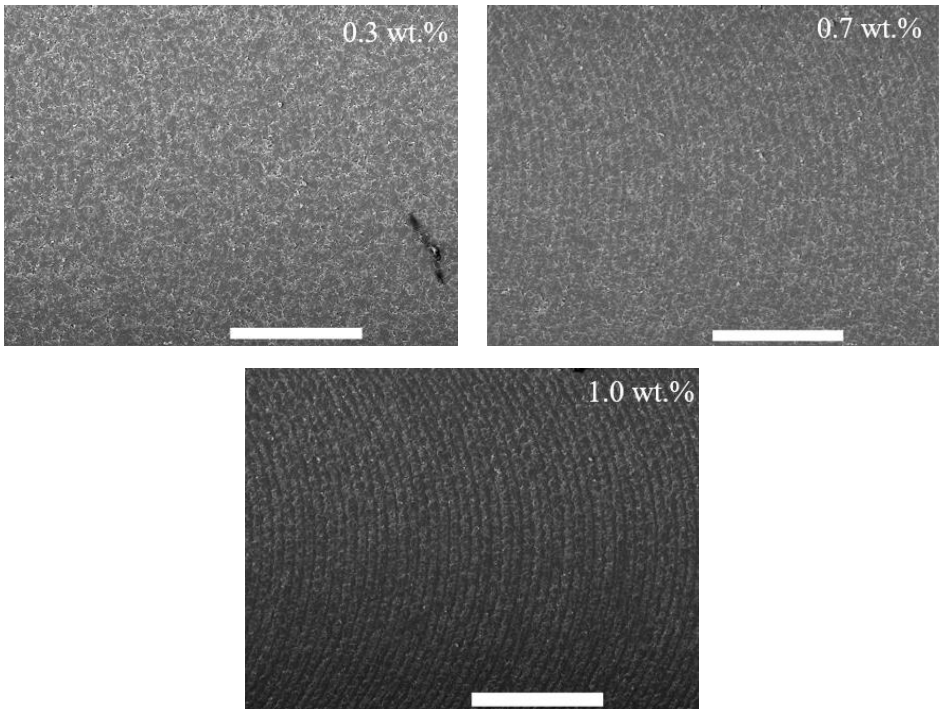

Figure 14: Surface morphology of machined surface at different CNT weight contents (FPT = 4 µm; Cutting speed = 62.8 m/min; Scale bar is 100 µm)

On closer investigation (Figure 15), other SEM images for all FPTs were taken at a higher magnification of 5kx. It was generally observed that the surface morphology from micro-milling higher filler content nanocomposites (0.7 wt.% and 1 wt.% MWCNT) tended to be smoother than those of the other compositions. The presences of cracks and crack ridges on their machined surfaces were also less frequent and prominent. It was likely due to MWCNT bridging the cracks that seemed to occur when high filler contents were employed. It has been confirmed by Samuel et al. [36] when micromachining PC/CNT nanocomposites. For plain epoxy, 0.1 and 0.3 wt.% MWCNT nanocomposites, machined surfaces seemed to be relatively smooth at the beginning (FPT from 0.2 to 0.5 µm) but became rougher with clear micro-cracks along with the feed marks when FPT increased, especially for 0.1 wt.% nanocomposites. It was possibly due to the effect of microstructure when the low interfacial strength of MWCT- epoxy making the fibres pull-out instead of being cut at 0.1 wt.% MWCNT. Polymer smearing of plain epoxy and partial CNT bridging of 0.3 wt.% MWCNT nanocomposites might contribute to their smoother surfaces compared to 0.1 wt.% counterpart. However, the machined surfaces of these materials appeared to be less rough as FPT reaching to 4 µm. The predominance of shearing regime might be the main reason for this. For micro-milling high-filler-content nanocomposites (0.7 and 1 wt.% MWCNT), the machined surfaces showed the evidence of the low-strain-failure effect that was seen in crack ridges as FPTs below MUCT. However, feed marks were much noticeable at FPT of 4 µm. It possibly led to higher surface roughness that indicated the main effect of feed rate at this cutting condition.

Overall, different surface morphologies have been observed for all material compositions. Tensile behaviour, microstructure and MUCT have shown significant influences on surface

morphology. These were confirmed through the discussion and SEM images. However, feed rate seemed to inconsiderably affect surface morphology while only clear feed marks were found at highest FPT. This claim should be confirmed by surface roughness measurements and its ANOVA analysis in section 3.7.

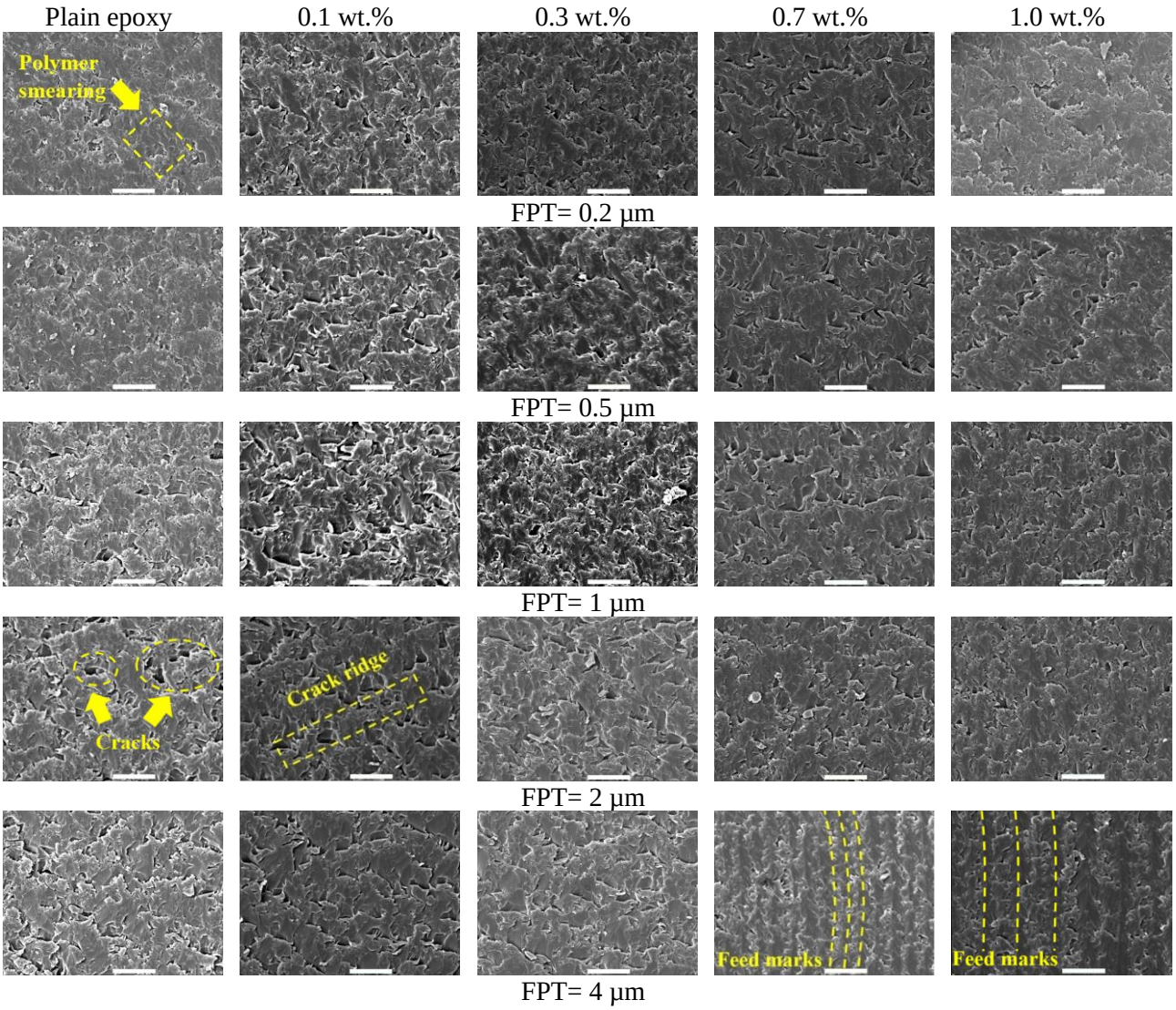

Figure 15: Surface morphology of machined surface at different CNT weight contents and FPTs (Cutting speed = 62.8 m/min; Scale bar is 10 µm)

3.7 Surface roughness

Before investigating surface roughness variation, ANOVA was first applied based on the experiment results from all cutting conditions and filler contents at a significance level (α) of 0.05. Table 3 shows all input factors, including filler content, cutting speed, and FPT with their effects on surface roughness representing as contribution indicators. It could be seen that filler content significantly affected the surface roughness with its contribution of ~30% followed by cutting speed (contribution of 25.69%) with their P-values below 0.001 while

FPT showed the least effect (2.46 5). These statistical results seemed to be consistent with the surface morphology analysis (section 3.6).

Table 3: ANOVA result for surface roughness when micro-milling epoxy/MWCNT nanocomposites

Source	DF	Seq SS	Contribution	Adj SS	Adj MS	F-Value	P-Value
Filler Content (wt.%)	4	0.061	30.50%	0.061	0.015	11.80	< 0.001
Cutting Speed (m/min)	2	0.051	25.69%	0.051	0.026	19.87	< 0.001
FPT (µm)	4	0.005	2.46%	0.005	0.001	0.95	0.440
Error	64	0.082	41.36%	0.082	0.001		
Total	74	0.199	100.00%				

Figure 16 depicts the surface roughness variation as a function of FPT at different filler contents. Surface roughness from micromachining 0.7 wt.% and 1 wt.% MWCNT nanocomposites were lower than the other composition regardless of the cutting conditions. It showed a firm agreement with the ANOVA analysis above. The Ra magnitudes of plain epoxy and other low-filler-content nanocomposites seemed to be comparable with each other, and their trends with FPT variations were also unclear indicating the minor effect of feed rate on surface roughness. However, from these figures (Figure 16), the effect of MUCT could be identified. In conventional machining, the increase of feed rate leads to the rise of surface roughness due to the effect of feed marks formation. In micromachining, when cutting below MUCT threshold, the ploughing mechanism occurs that may have negative impacts on machined surface generation. From this study, it was seen that for all cutting conditions, surface roughness fluctuated along with FPT. As FPT increasing from 0.2 to 1 µm which was below MUCT (as indicated by chip morphology and cutting force discussion), there was a fluctuation of surface roughness with high magnitudes at the beginning due to ploughing. It then reached to the bottom at FPT = 0.5 µm with ploughing-shearing and then increased again as FPT reached to 1 µm when a shearing regime becomes more dominant.

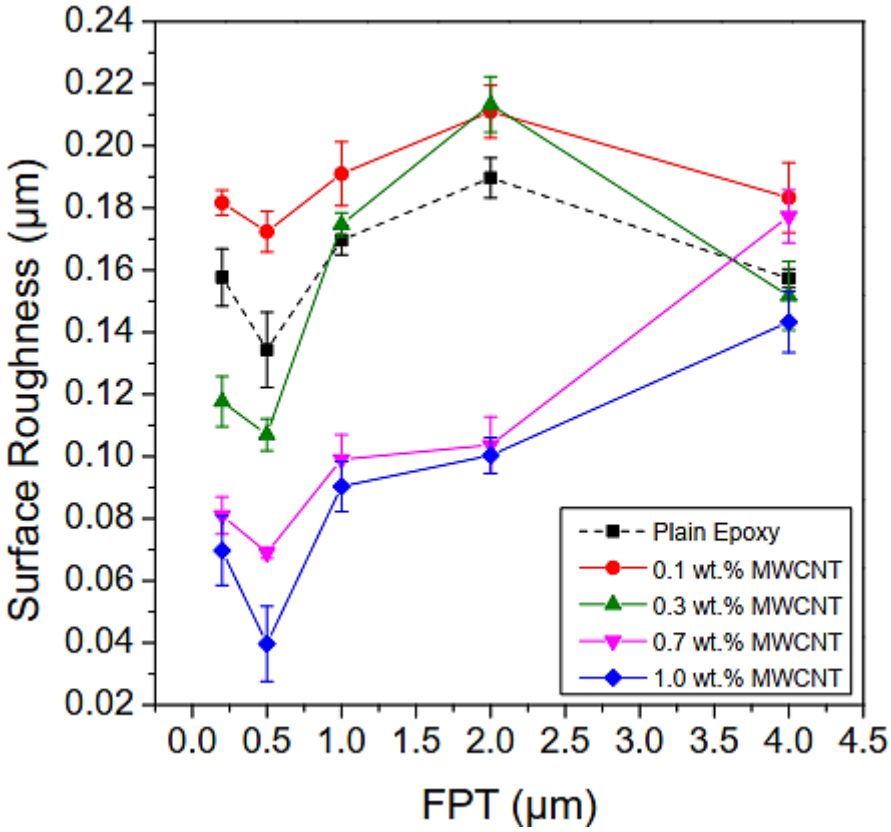

Figure 16: Surface roughness (Ra) when micro-milling epoxy-based nanocomposites at different MWCNT contents and FPTs (cutting speed = 62.8 m/min)

A fluctuation of Ra could be seen for all materials as FPT increasing up to 1 µm. As indicated by chip morphology investigation, this range of FPT was still below MUCT (below 2 µm) for these nanocomposites, hence showing the impact of the size effect. A continuous decrease of Ra at the beginning was possibly responsible for partial ploughing, therefore mostly having no shearing at this stage. When the FPT kept increasing into 4 µm, the dominance feed mark effect was now responsible for the significant increase of Ra. However, the surface roughness of epoxy and low filler content nanocomposites (0.1 wt.% and 0.3 wt.%) started to decrease when FPR reaches to 2 µm. More polymer smearing due to high cutting temperature at high feed rates might be the reason for this phenomenon.

3.8 Tool wear

Figure 17 shows the side and top views of machined micro-end mill for all material compositions to depict the effect of workpiece properties on the flank wear and the face wear, respectively. These two wear patterns seemed to be only visible at high filler contents (0.7 and 1 wt.%).This phenomenon was confirmed by the results of tool wear measurements (Figure 18). For low filler content compositions and plain epoxy, there was unobvious effect of filler contents on the tool wear. However, an increase from 0.7 to 1 wt.% MWCNT content exhibited considerable tool wear acceleration, especially flank wear. It was exhibited by the visible scratches on the tool flank face when micro-milling these compositions (Figure 17).

Given such high filler loadings of MWCNT, it likely indicated more physical contact between the tools and nano-fibres, hence resulting in more tool wear. Additionally, MWCNT agglomeration at high filler loadings might also contribute to more trapping between tool and workpiece, caused more tool wear due to rubbing. This claim was supported by the stack of MWCNTs adhered on the tool surfaces when machined 0.7 and 1 wt.% nanocomposites (Figure 17).

In addition, the apparent melting chip adhesion on the flank face could be seen for the micro-tools which machined epoxy and low filler-content nanocomposites (0.1 and 0.3 w.t%). It possibly indicated the effect of thermal softening when micromachining these low-thermal-conductivity materials. On the other hand, the chips adhered on the tool surfaces when machined high-filler-content compositions (0.7 and 1 w.t%) were in discontinuous form, implying the high brittleness of these nanocomposites. Also, their high thermal conductivity might contribute to the reduction of thermal softening, hence resulting in less melting chip adhesion.

Filler content	Side view (Scale bar is 50 µm)	Top View (Scale bar length 10 µm)
Plain epoxy	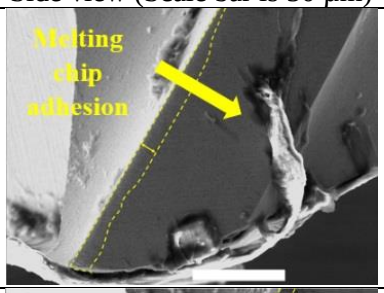	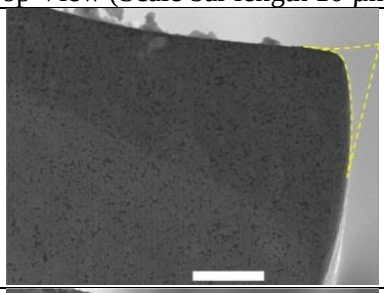
0.1 wt%	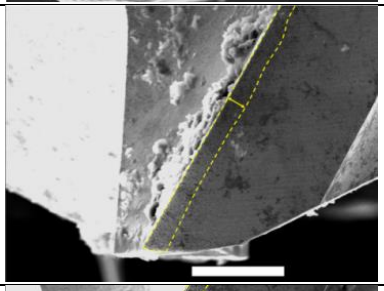	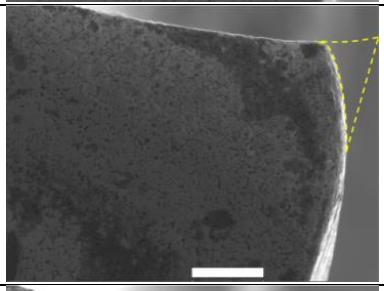
0.3 wt%	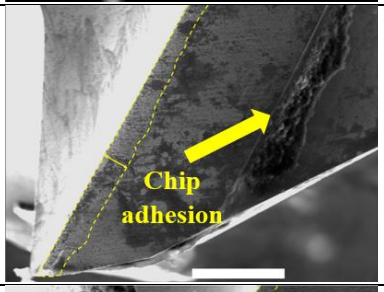	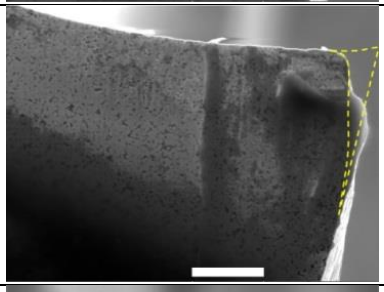
0.7 wt%	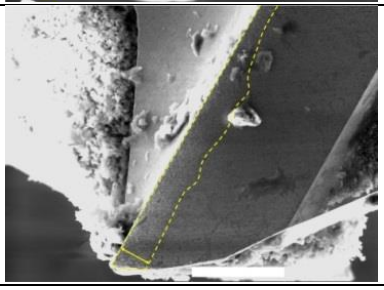	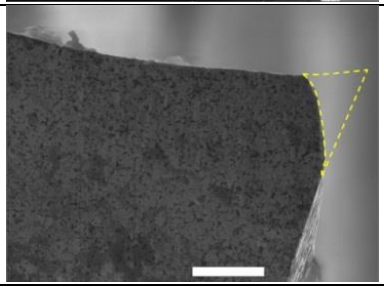

1.0 wt%	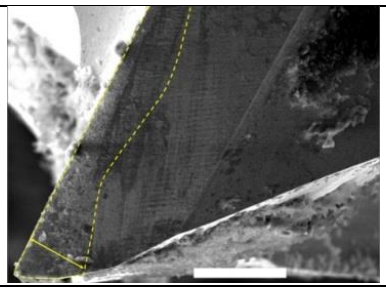	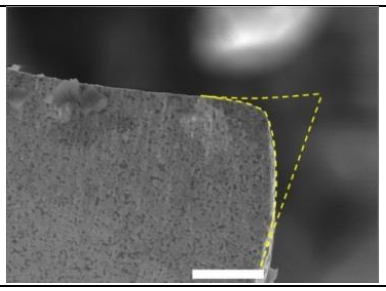

Figure 17: SEM images of tool wear at the end of the micro-milling process for each composition (cutting volume of 58.5 mm3) (Yellow dashed line indicating wear area)

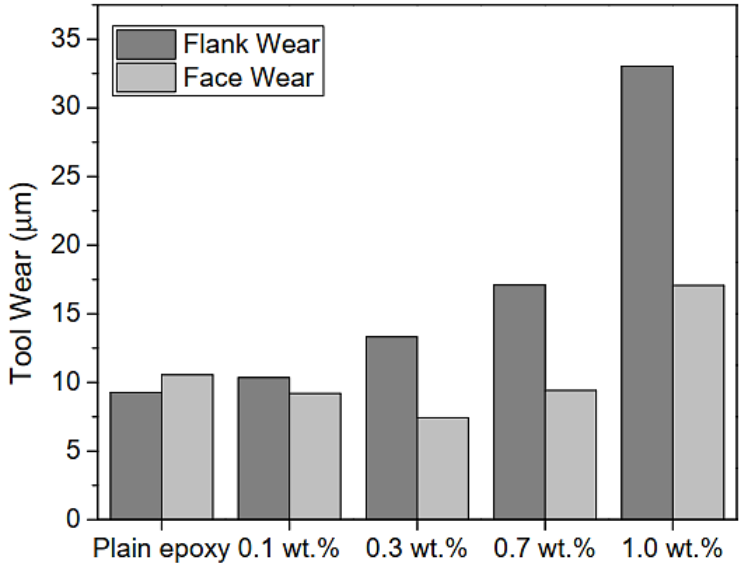

Figure 18: Effect of MWCNT content on tool wear when micro-milling epoxy/MWCNT nanocomposites

4. Conclusions

The micro-machinability of multi-walled carbon nanotube reinforced epoxy nanocomposites (epoxy/MWCNT) was experimentally investigated and compared to those of plain epoxy with the consideration of size effect. The variations of cutting force and surface roughness were investigation with the validation from chip formation, surface morphology as well as workpiece material properties (mechanical tensile properties and thermal conductivity). Additionally, the influences of other factors including thermal softening, mechanical strengthening, micro-structure, ploughing-shearing from MUCT or size effect were also addressed. Nevertheless, within the scope of this paper, some main conclusions could be drawn:

a. MWCNT content was the most critical factor affecting the micro-milling machinability of epoxy/MWCNT nanocomposites in terms of cutting force, surface roughness and tool wear. It indicated the main effects of microstructure as well as the correlation of mechanical strengthening - thermal softening dominant regimes. This aspect has been confirmed and

linked to mechanical tensile properties and thermal conductivity characterisation of the materials.

b. Feed rate had the most effect on cutting force variation. Its acceleration significantly led to an apparent upward trend of cutting force when micromachining at feed rates beyond MUCT that was similar to that of macro-machining. On the other hand, the size effect dominated at lower FPTs, indicating by a fluctuation of cutting force at this range of feed rate.

c. Cutting speed showed its considerable influence on surface roughness generation. Rougher machined surfaces could be seen as cutting speed increasing, indicating a converse trend compared to that of macro-machining. Thermal-softening associated with polymer-negative effects might negatively contribute to an upward trend of surface roughness in this case.

d. The size effect was likely to appear when micro-milling of epoxy/MWCNT nanocomposites at FPT below MUCT threshold. It exhibited by the fluctuations of both cutting speed and surface roughness at low chip loads due to the transition from ploughing to shearing cutting regime. The MUCT value varies between different workpiece materials, owing by their various tensile behaviours (i.e., fracture strain). The addition of high MWCNT content (0.7 and 1 wt.%) led to a reduction of MUCT compared to other low-filler-content compositions.

References

[1] B. Han, S. Sun, S. Ding, L. Zhang, X. Yu, and J. Ou, "Review of nanocarbon-engineered multifunctional cementitious composites," *Composites Part A: Applied Science and Manufacturing,* vol. 70, pp. 69-81, 2015.

[2] X.-L. Xie, Y.-W. Mai, and X.-P. Zhou, "Dispersion and alignment of carbon nanotubes in polymer matrix: a review," *Materials science and engineering: R: Reports,* vol. 49, pp. 89-112, 2005.

[3] S. Iijima, "Helical microtubules of graphitic carbon," *nature,* vol. 354, pp. 56-58, 1991.

[4] S. Iijima and T. Ichihashi, "Single-shell carbon nanotubes of 1-nm diameter," *nature,* vol. 363, pp. 603-605, 1993.

[5] B. Singh, C. Baburao, V. Pispati, H. Pathipati, N. Muthy, S. Prassana*, et al.*, "Carbon nanotubes. A novel drug delivery system," *International Journal of Research in Pharmacy and Chemistry,* vol. 2, pp. 523-532, 2012.

[6] S. Kumar, R. Rani, N. Dilbaghi, K. Tankeshwar, and K.-H. Kim, "Carbon nanotubes: a novel material for multifaceted applications in human healthcare," *Chemical society reviews,* vol. 46, pp. 158-196, 2017.

[7] L.-M. Peng, Z. Zhang, and S. Wang, "Carbon nanotube electronics: recent advances," *Materials today,* vol. 17, pp. 433-442, 2014.

[8] M. F. De Volder, S. H. Tawfick, R. H. Baughman, and A. J. Hart, "Carbon nanotubes: present and future commercial applications," *science,* vol. 339, pp. 535-539, 2013.

[9] A. Toldy, B. Szolnoki, and G. Marosi, "Flame retardancy of fibre-reinforced epoxy resin composites for aerospace applications," *Polymer degradation and stability,* vol. 96, pp. 371-376, 2011.

[10] A. K. Naskar, J. K. Keum, and R. G. Boeman, "Polymer matrix nanocomposites for automotive structural components," *Nature nanotechnology,* vol. 11, pp. 1026-1030, 2016.

[11] C. Chen, Y. Xue, X. Li, Y. Wen, J. Liu, Z. Xue*, et al.*, "High-performance epoxy/binary spherical alumina composite as underfill material for electronic packaging," *Composites Part A: Applied Science and Manufacturing,* vol. 118, pp. 67-74, 2019.

[12] K. A. Muhammed, C. R. Kannan, B. Stalin, and M. Ravichandran, "Experimental investigation on AW 106 Epoxy/E-Glass fiber/nano clay composite for wind turbine blade," *Materials Today: Proceedings,* vol. 21, pp. 202-205, 2020.
[13] E. Yusup, S. Mahzan, and M. Kamaruddin, "Natural Fiber Reinforced Polymer for the Application of Sports Equipment using Mold Casting Method," in *IOP Conference Series: Materials Science and Engineering*, 2019, p. 012040.
[14] H. Cebeci, R. G. de Villoria, A. J. Hart, and B. L. Wardle, "Multifunctional properties of high volume fraction aligned carbon nanotube polymer composites with controlled morphology," *Composites Science and Technology,* vol. 69, pp. 2649-2656, 2009.
[15] A. Allaoui, S. Bai, H.-M. Cheng, and J. Bai, "Mechanical and electrical properties of a MWNT/epoxy composite," *Composites science and technology,* vol. 62, pp. 1993-1998, 2002.
[16] M. Loos, *Carbon nanotube reinforced composites: CNT Polymer Science and Technology*: Elsevier, 2014.
[17] M. Anis, G. AlTaher, W. Sarhan, and M. Elsemary, "Sports Equipment," in *Nanovate*, ed: Springer, 2017, pp. 183-192.
[18] T. Hayashi and M. Endo, "Carbon nanotubes as structural material and their application in composites," *Composites Part B: Engineering,* vol. 42, pp. 2151-2157, 2011.
[19] B. Le, J. Khaliq, D. Huo, X. Teng, and I. Shyha, "A Review on Nanocomposites. Part 1: Mechanical Properties," *Journal of Manufacturing Science and Engineering,* vol. 142, 2020.
[20] B. Le, J. Khaliq, D. Huo, X. Teng, and I. Shyha, "A Review on Nanocomposites. Part 2: Micromachining," *Journal of Manufacturing Science and Engineering,* vol. 142, 2020.
[21] X. Xin, M. Liang, Z. Yao, L. Su, J. Zhang, P. Li*, et al.*, "Self-sensing behavior and mechanical properties of carbon nanotubes/epoxy resin composite for asphalt pavement strain monitoring," *Construction and Building Materials,* vol. 257, p. 119404, 2020.
[22] D. Kumar, T. Goyal, V. Kumar, P. Mohite, S. Kamle, and V. Verma, "Development and modal analysis of bioinspired CNT/epoxy nanocomposite MAV flapping wings," *J. Aerosp. Sci. Technol,* vol. 67, pp. 88-93, 2015.
[23] N. Shakoori, G. Fu, B. Le, J. Khaliq, L. Jiang, D. Huo*, et al.*, "An experimental investigation on tool wear behaviour of uncoated and coated micro-tools in micro-milling of graphene-reinforced polymer nanocomposites," *The International Journal of Advanced Manufacturing Technology,* vol. 113, pp. 2003-2015, 2021.
[24] J. Samuel, A. Dikshit, R. E. DeVor, S. G. Kapoor, and K. J. Hsia, "Effect of carbon nanotube (CNT) loading on the thermomechanical properties and the machinability of CNT-reinforced polymer composites," *Journal of Manufacturing Science and Engineering,* vol. 131, 2009.
[25] M. Mahmoodi, M. Mostofa, M. Jun, and S. S. Park, "Characterization and micromilling of flow induced aligned carbon nanotube nanocomposites," *Journal of Micro and Nano-Manufacturing,* vol. 1, 2013.
[26] M. N. Kumar, M. Mahmoodi, M. TabkhPaz, S. Park, and X. Jin, "Characterization and micro end milling of graphene nano platelet and carbon nanotube filled nanocomposites," *Journal of Materials Processing Technology,* vol. 249, pp. 96-107, 2017.
[27] I. Arora, J. Samuel, and N. Koratkar, "Experimental investigation of the machinability of epoxy reinforced with graphene platelets," *Journal of Manufacturing Science and Engineering,* vol. 135, 2013.
[28] I. Shyha, G. Y. Fu, D. H. Huo, B. Le, F. Inam, M. S. Saharudin*, et al.*, "Micro-machining of nano-polymer composites reinforced with graphene and nano-clay fillers," in *Key Engineering Materials*, 2018, pp. 197-205.
[29] "Tool Life Testing in Milling - Part 2: End Milling," *International Standards Organisation,* vol. ISO 8688-2, 1989.

601 [30] "Geometrical Product Specifications (GPS) — Surface texture: Profile method — Terms, definitions
602 and surface texture parameters," *International Standards Organisation,* vol. ISO 4287:1997, 1997.
603 [31] A. T. Seyhan, M. Tanoğlu, and K. Schulte, "Tensile mechanical behavior and fracture toughness of
604 MWCNT and DWCNT modified vinyl-ester/polyester hybrid nanocomposites produced by 3-roll
605 milling," *Materials Science and Engineering: A,* vol. 523, pp. 85-92, 2009.
606 [32] B. K. Satapathy, R. Weidisch, P. Pötschke, and A. Janke, "Tough-to-brittle transition in multiwalled
607 carbon nanotube (MWNT)/polycarbonate nanocomposites," *Composites science and technology,*
608 vol. 67, pp. 867-879, 2007.
609 [33] F. Gardea and D. C. Lagoudas, "Characterization of electrical and thermal properties of carbon
610 nanotube/epoxy composites," *Composites Part B: Engineering,* vol. 56, pp. 611-620, 2014.
611 [34] F. H. Gojny, M. H. Wichmann, B. Fiedler, I. A. Kinloch, W. Bauhofer, A. H. Windle*, et al.*, "Evaluation
612 and identification of electrical and thermal conduction mechanisms in carbon nanotube/epoxy
613 composites," *Polymer,* vol. 47, pp. 2036-2045, 2006.
614 [35] S.-Y. Yang, C.-C. M. Ma, C.-C. Teng, Y.-W. Huang, S.-H. Liao, Y.-L. Huang*, et al.*, "Effect of
615 functionalized carbon nanotubes on the thermal conductivity of epoxy composites," *Carbon,* vol.
616 48, pp. 592-603, 2010.
617 [36] J. Samuel, A. Dikshit, R. E. DeVor, S. G. Kapoor, and K. J. Hsia, "Effect of carbon nanotube (CNT)
618 loading on the thermomechanical properties and the machinability of CNT-reinforced polymer
619 composites," *Journal of Manufacturing Science and Engineering,* vol. 131, p. 031008, 2009.

620